



REPORT

NOD is a plus end-directed motor that binds EB1 via a new microtubule tip localization sequence

Anna A. Ye^{1,2} , Vikash Verma¹, and Thomas J. Maresca^{1,2} 

Chromosome congression, the process of positioning chromosomes in the midspindle, promotes the stable transmission of the genome to daughter cells during cell division. Congression is typically facilitated by DNA-associated, microtubule (MT) plus end-directed motors called chromokinesins. The *Drosophila melanogaster* chromokinesin NOD contributes to congression, but the means by which it does so are unknown in large part because NOD has been classified as a nonmotile, orphan kinesin. It has been postulated that NOD promotes congression, not by conventional plus end-directed motility, but by harnessing polymerization forces by end-tracking on growing MT plus ends via a mechanism that is also uncertain. Here, for the first time, it is demonstrated that NOD possesses MT plus end-directed motility. Furthermore, NOD directly binds EB1 through unconventional EB1-interaction motifs that are similar to a newly characterized MT tip localization sequence. We propose NOD produces congression forces by MT plus end-directed motility and tip-tracking on polymerizing MT plus ends via association with EB1.

Introduction

Equal distribution of duplicated DNA is required to maintain genomic stability through cell division. The microtubule (MT) cytoskeleton is reorganized to form a bipolar spindle as cells enter mitosis or meiosis. Chromosomes are positioned at the spindle equator during a process known as congression. Chromosome movements within the spindle are predominantly mediated by motor proteins that walk directionally on spindle MTs. An important class of congression motors is the chromokinesins, which include the kinesin families, kinesin-4, kinesin-10, and kinesin-12. Chromokinesins work cooperatively to promote chromosome alignment during cell division (Goshima and Vale, 2003; Stumpff et al., 2012; Wandke et al., 2012). Kinesin-10 and kinesin-4 are chromosome-associated, plus end-directed motors, although KIF4A suppresses plus end MT dynamics (Bringmann et al., 2004; Hu et al., 2011; Stumpff et al., 2012) and may dampen polar ejection forces (PEFs) that push chromosome arms away from spindle poles, whereas kinesin-10's role is more intuitive and likely the predominant PEF-producing motor. The function of vertebrate kinesin-10 (Kid) was first described in *Xenopus laevis* egg extracts in which Xkid was required to establish and maintain chromosome arm congression (Antonio et al., 2000; Funabiki and Murray, 2000; Takagi et al., 2013). Although data from human cells have consistently shown that hKid contributes to congression, the alignment defects observed in tissue culture

cells have not been as severe as in egg extracts (Levesque and Compton, 2001; Tokai-Nishizumi et al., 2005; Stumpff et al., 2012; Wandke et al., 2012). Vertebrate kinesin-10s have been shown to possess plus end-directed motility and to generate force when bound to chromatin (Yajima et al., 2003; Brouhard and Hunt, 2005; Bieling et al., 2010; Stumpff et al., 2012).

The *Drosophila melanogaster* chromokinesin NOD shares sequence homology in its N-terminal motor with both kinesin-10 and kinesin-4 motor domains and in its C terminus with the kinesin-10 DNA-binding motif (helix-hairpin-helix), but it has been designated an orphan kinesin as a result of significant divergence in its structural elements and organization relative to conventional kinesins (Goldstein, 1993; Matthies et al., 2001). NOD was initially identified and characterized genetically as the mutant no distributive disjunction (*nod*), which exhibited high frequencies of nondisjunction and chromosome loss in female meiosis (Carpenter, 1973; Zhang and Hawley, 1990). The *nod* gene encodes a kinesin-like protein (NOD) with an N-terminal motor domain (Zhang et al., 1990). Achiasmate (nonexchange) chromosomes frequently failed to associate with spindles or were mispositioned near spindle poles in oocytes lacking functional NOD (Theurkauf and Hawley, 1992). The characterization of DNA binding activities in the C terminus of NOD (Afshar et al., 1995b; Cui and Hawley, 2005), its N-terminal motor domain, and the

¹Biology Department, University of Massachusetts, Amherst, Amherst, MA; ²Molecular and Cellular Biology Graduate Program, University of Massachusetts, Amherst, Amherst, MA.

Correspondence to Thomas J. Maresca: tmaresca@bio.umass.edu.

© 2018 Ye et al. This article is distributed under the terms of an Attribution–Noncommercial–Share Alike–No Mirror Sites license for the first six months after the publication date (see <http://www.rupress.org/terms/>). After six months it is available under a Creative Commons License (Attribution–Noncommercial–Share Alike 4.0 International license, as described at <https://creativecommons.org/licenses/by-nc-sa/4.0/>).

misalignment phenotype of *nod* mutants led to the hypothesis that NOD is the PEF motor in fly oocytes (Afshar et al., 1995a), and later work in *Drosophila* tissue culture cells revealed a role for NOD in mitotic chromosome congression (Goshima and Vale, 2003). Although NOD possesses a conserved N-terminal motor domain and MT-stimulated ATPase activity, efforts to reconstitute directional motility in vitro have failed (Matthies et al., 2001) leading to NOD being classified as a nonmotile kinesin. How could a nonmotile kinesin generate force? An alternative theory posits that, as a result of the unique mechanochemical properties of its motor domain, NOD moves chromosomes by associating with the plus ends of polymerizing MTs (Cui et al., 2005; Cochran et al., 2009), although direct evidence for this mechanism is lacking. High resolution imaging of NOD-coated chromatin stretching events in living cells were suggestive of both plus end-directed motility and end-tracking coincident with EB1 comets (Cane et al., 2013).

Results and discussion

NOD possesses an N-terminal motor domain and two distinct C-terminal DNA binding regions comprised of high mobility group (HMG) repeats and a helix-hairpin-helix motif that mediate chromatin-association of full length (FL) NOD-mCherry throughout the cell cycle in *Drosophila* S2 cells (Fig. 1, A and B). Between the motor and DNA-binding domains, NOD is predicted to contain intrinsically disordered regions (~50%), as well as four α -helices, one of which has a low probability of forming a parallel two-stranded coiled coil (CC; Lupas et al., 1991; Buchan et al., 2013). To dissect NOD motor function in vivo, truncations of NOD tagged at their C termini with mCherry were expressed in GFP- α -tubulin expressing *Drosophila* S2 cells (Fig. 1 C). The motor domain (1–324) did not bind MTs in mitosis or interphase and was diffuse in the cytosol. Thus, unlike many well-characterized motor proteins, the NOD324 motor domain exhibits weak or no MT binding activity in cells. Given the high physiological concentration of ATP, this observation is consistent with in vitro studies in which NOD motor domain exhibited significantly lower MT binding affinities in the presence of excess ATP than conventional kinesin motors (Matthies et al., 2001; Cochran et al., 2009).

Most kinesins with N-terminal motor domains possess a neck linker and a well-defined neck CC downstream of the motor; however, some kinesins, including NOD, have noncanonical neck regions that contribute to their functions in cells (Davies et al., 2015). We next examined the localization of a NOD truncation (1–485) that encompasses the motor domain and the noncanonical neck extension region. Addition of the neck extension conferred MT-binding activity in cells as NOD485 uniformly coated MTs throughout the cell cycle (Fig. 1 C). Inclusion of the nonconventional extension could promote MT binding through numerous nonexclusive mechanisms, including the introduction of a second MT binding site, which has been shown for hKID (Shiroguchi et al., 2003), posttranslational modifications, association with regulatory factors, or dimerization through the low probability CC. The MT localization of NOD485 was significantly reduced upon fixation conditions suggestive of the

interaction, while stronger than NOD324, being relatively low affinity (Table 1). Nonetheless, the localization of NOD485 led us to reason that the oligomeric state of NOD warranted further investigation. Several structural and functional aspects of NOD are reminiscent of the monomeric plus end-directed kinesin Unc104/KIF1A. Kinesin-10 family members have been shown to be monomeric in vitro (Shiroguchi et al., 2003). Furthermore, NOD and Unc104/KIF1A possess low-probability/weak CC regions adjacent to their N-terminal motors, whereas their C termini contain domains that cluster the motors on the surface of cargos: chromosomes and synaptic vesicles, respectively (Klopfenstein et al., 2002; Klopfenstein and Vale, 2004). Prior work on Unc104 demonstrated that constitutive dimerization of the Unc104 motor domain and its adjacent “weak” CC converted the monomer into a processive, plus end-directed motor with physiological velocities (Tomishige et al., 2002). A comparable approach as that applied to Unc104, specifically fusion to the kinesin-1 “stalk” CC, was next used to examine how dimerization of the NOD motor domain affected its behavior (Fig. 1 A).

The motor domain alone (1–324) was first dimerized. NOD324CC evenly coated interphase MTs and robustly associated with spindle MTs during mitosis, exhibiting a slight enrichment toward the plus ends of kinetochore fibers in the vicinity of aligned chromosomes with some evident MT bundling (Fig. 1 C). NOD485CC exhibited a striking localization pattern in which it was highly enriched near MT plus ends in mitosis and interphase. Significant MT bundling was also observed throughout the cell cycle especially in cells with high NOD485CC levels, which was not observed in the NOD485-expressing cells (Fig. 1 C). The localization patterns and behavior of the dimerized NOD truncations were not attributable to the kinesin-1 CC because CC-mCherry only weakly associated with a subset of MTs in some cells and exhibited no obvious or consistent localization pattern. Furthermore, the neck extension region, while necessary, was not sufficient for MT binding, as the localization patterns of NOD325–485 and NOD325–485CC were identical to mCherry and CC-mCherry, respectively (Table 1).

The localization pattern of NOD485CC suggested dimerized NOD could possess plus end-directed motility in cells. This possibility was further examined by imaging cells using total internal reflection fluorescence (TIRF) microscopy to visualize NOD on the MTs closest to the cell cortex. Puncta of both NOD485 and NOD324CC were visible on MTs, but motility was not obvious (Table 1). The behavior of NOD485CC was markedly different from the other truncations as NOD puncta were clearly observed moving processively on MTs toward the cell periphery (Fig. 2, A–C; and Video 1). The distribution of fluorescence intensities of motile NOD485CC-mCherry puncta was indistinguishable from that of motile kinesin-1-mCherry dimers, demonstrating that NOD485CC was assembling into motile dimers (Fig. S1). Measurements of motile NOD485CC dimers in cells yielded a mean velocity of $8.70 \pm 3.61 \mu\text{m}/\text{min}$ (mean \pm SD is reported for all motility measurements; Fig. 2 D). These data demonstrate that dimerization of the NOD motor domain alone (NOD324CC) promotes MT binding but not motility, most likely because it lacks a functional neck linker, which plays an important role in coordinating motor head functions (Vale and Milligan, 2000), whereas

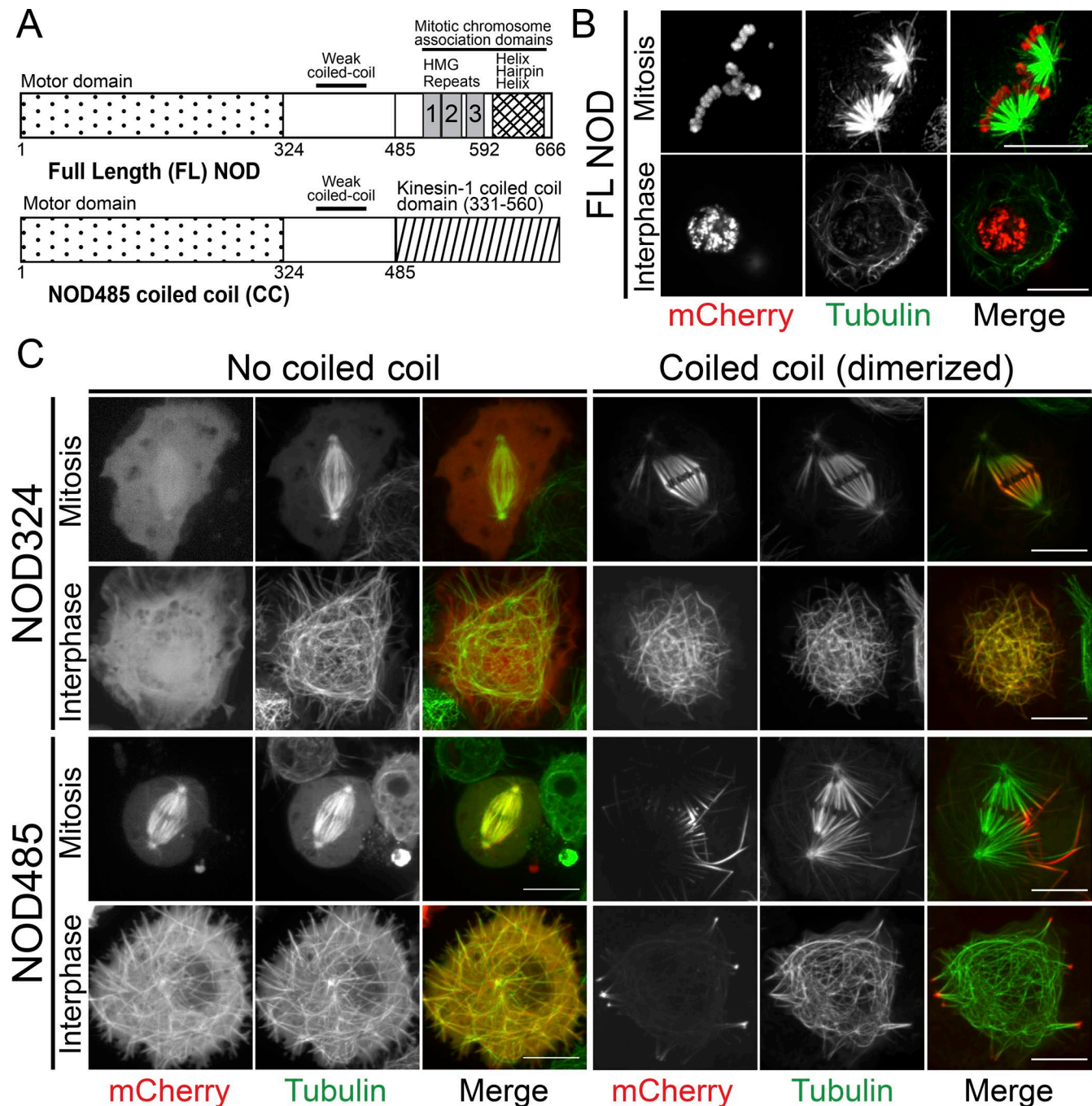


Figure 1. The motor domain and nonconventional neck structure of NOD are required for MT binding and become enriched at MT plus ends when dimerized. (A) Schematics of the FL NOD and dimerized NOD485CC. **(B)** Maximum projections of two-color spinning disc confocal images showing the chromosomal localization of FL NOD overexpressed in *Drosophila* S2 cells. **(C)** Maximum projections of two-color spinning disc confocal images of *Drosophila* S2 cells expressing NOD motor domain (NOD324) and a NOD truncation including the motor and neck extension region (NOD485) plus and minus the dimerizing CC. NOD is shown in red; tubulin is shown in green. Bars, 10 μ m.

dimerization of the motor domain and nonconventional neck extension region converts NOD into a directional motor.

To further characterize NOD motility in vitro, we applied TIRF-based imaging to cell extracts (Cai et al., 2007; Mann et al., 2017) in which NOD485CC was the only fluorescently tagged component. Using this technique, NOD motility could be studied in near physiological conditions, but in a chamber in which the state of the MTs, which are attached to the cover-glass, as well as the

buffering conditions can be controlled. In cell lysates prepared from NOD485CC-expressing cells, NOD walked unidirectionally on taxol stabilized MTs in an ATP-dependent manner (Fig. 2 E and F; and Videos 2 and 3). The mean velocity of $8.62 \pm 2.32 \mu\text{m}/\text{min}$ measured for motile NOD485CC dimers in cell lysates was indistinguishable from live-cell measurements (Fig. 2, D and F).

NOD motility has never been reconstituted in vitro and, like others, we were unable to purify active NOD485CC from bacteria.

Table 1. Summary of NOD localizations and activities

	MT association	Plus end-directed motility	Plus end tracking
NOD324	-	-	-
NOD324CC	++	-	-
NOD485	+	-	-
NOD485CC	++	+	+
NOD325-485	-	-	-
NOD325-485-CC	±	-	-
Kinesin-1 CC	±	-	-

CC, Kinesin-1 CC domain; -, not observed; ±, weak and variable localization to a subset of MTs; +, weak association; ++, strong association. Classifications were determined by live cell imaging. The ± constructs were designated as variable because they weakly localized to a subset of apparently bundled MTs in some interphase cells. MT association of NOD485 was designated as weak (+) because it was not retained after fixation with paraformaldehyde and permeabilization with detergent during preparations for immunofluorescence.

Furthermore, NOD485CC activity in cell lysates was labile and sensitive to buffer conditions. Thus, NOD485CC-mCherry was purified from *Drosophila* S2 cells using a C-terminal Strep tag that allows for affinity purification on a streptavidin-based matrix and gentle elution using biotin-containing buffers to better preserve protein activity. Silver staining of the purification revealed a unique band, when compared with a mock purification from wild-type cell extracts, at the predicted size of NOD485CC-mCherry (~110 kD), which was confirmed by Western blot using an mCherry antibody (Fig. 2 I). Although it is probable that NOD-associated proteins were copurified in the preparation, the majority of background bands were likely biotinylated proteins or nonspecific because a nearly identical banding pattern was observed in mock purifications from wild-type cell extracts (Fig. 2 I). In TIRF assays, the affinity purified NOD485CC-mCherry exhibited ATP-dependent, unidirectional motility, although the mean velocity of $5.79 \pm 1.56 \mu\text{m}/\text{min}$ was slower than velocities measured in cells and lysates (Fig. 2, G and H; and Videos 4 and 5).

NOD485CC dimers often moved toward the cell periphery where the MT plus ends are typically oriented during interphase. To define the directionality of NOD485CC motility, purified GFP-labeled human kinesin-1 (Kif5B) motor, a plus end-directed motor, was added to lysates from NOD485CC-mCherry expressing cells. NOD485CC and kinesin-1 walked in the same direction, establishing that NOD is a plus end-directed motor (Fig. 2 J and Video 6). Collectively, the data in cells and in vitro demonstrate that dimerized NOD is a plus end-directed motor with velocities similar to those measured for Xkid and hKID (Yajima et al., 2003; Brouhard and Hunt, 2005; Bieling et al., 2010), which in combination with the presence of a C-terminal helix-hairpin-helix DNA-binding motif warrants consideration of NOD as the *Drosophila* kinesin-10 orthologue.

We next tested if chemically induced dimerization was sufficient to support NOD motility by building cell lines coexpressing dark (no fluorescent tag) NOD485-FRB and NOD485-FKBP-EGFP (Fig. 3 A). Like NOD485, NOD485-FKBP-EGFP localized uniformly to MTs in the absence of rapamycin. Upon addition of 100 nM rapamycin, motile puncta of NOD485-FKBP-EGFP moved on MTs toward the cell periphery (Fig. 3, B–D; and Video 7). Extracts were next prepared from NOD485-FKBP-EGFP, NOD485-FRB-expressing cells to visualize NOD on MTs by TIRF microscopy in vitro. Without rapamycin, nonmotile puncta of NOD485-FKBP-EGFP associated with MTs (Fig. 3 E and Video 8). Unidirectional motility of NOD485-FKBP-EGFP puncta was achieved within minutes of adding 100 nM rapamycin to the same cell extracts that did not exhibit motility in the absence of rapamycin (Fig. 3 F and Video 9). Cell lines coexpressing NOD485-FKBP-EGFP and NOD485-FRB-mCherry (Fig. 3 G) were next visualized. In the absence of rapamycin, the mCherry and EGFP-tagged NOD uniformly coated the MTs similar to NOD485, but NOD localization changed upon addition of 100 nM rapamycin as EGFP- and mCherry-tagged, chemically dimerized NOD485 accumulated toward MT plus ends at the cell periphery similar to NOD485CC (Fig. 3 H). Altogether, the kinesin-1 CC and chemically induced dimerization data support the conclusion that multiple modes of NOD485 dimerization can support directional motility.

Although earlier work visualizing MT-associated stretching of NOD-coated chromatin was indicative of plus end-directed motility (Cane et al., 2013), it is technically challenging to assess the activity of nonartificially dimerized NOD in cells as a result of its constitutive chromatin localization. Fortunately, NOD contains an endogenous nuclear export signal (NES) computationally predicted and borne out by the localization of various NOD truncations (unpublished data). Although NOD possesses an NES, it is not typically observed in the cytosol because it is tightly associated with chromatin throughout the cell cycle. We reasoned that the affinity of NOD for chromatin could be reduced by deleting one of its two chromosome-associating domains (HMG14/17 repeats), a truncation we called NODΔHMG (Fig. 3 I). In ~10% of cells expressing NODΔHMG, possibly as a result of reduced affinity for the chromatin and the presence of an NES, cytosolic NOD puncta were visible. Therefore, we were able to visualize nearly FL cytosolic NOD that was not artificially dimerized with CC or FKBP-FRB domains. Importantly, the cytosolic NODΔHMG exhibited plus end-directed motility toward the cell periphery along interphase MTs (Fig. 3, J and K; and Videos 10 and 11). Compared with the kinesin-1-mCherry standard, motile NODΔHMG puncta spanned a range of fluorescence intensities corresponding to ~5–200 NOD molecules with a mean of 52 motors per puncta, suggesting that NOD may function as clusters of dimers or more complex oligomers (Fig. S1, B and C). Nevertheless, the velocity of NODΔHMG clusters (Fig. 3 L) was comparable to the velocities measured for NOD485CC dimers in cells and cell lysates in vitro ($7.6 \mu\text{m}/\text{min}$ for NODΔHMG in cells vs. 8.6 – $8.7 \mu\text{m}/\text{min}$ for NOD485CC in cells and lysates).

Prior work characterized NOD-coated chromatin stretch events that colocalized with EB1 comets, as well as occasional cytoplasmic NOD fragments that tracked polymerizing and depolymerizing MT plus ends (Cane et al., 2013), and NODΔHMG puncta

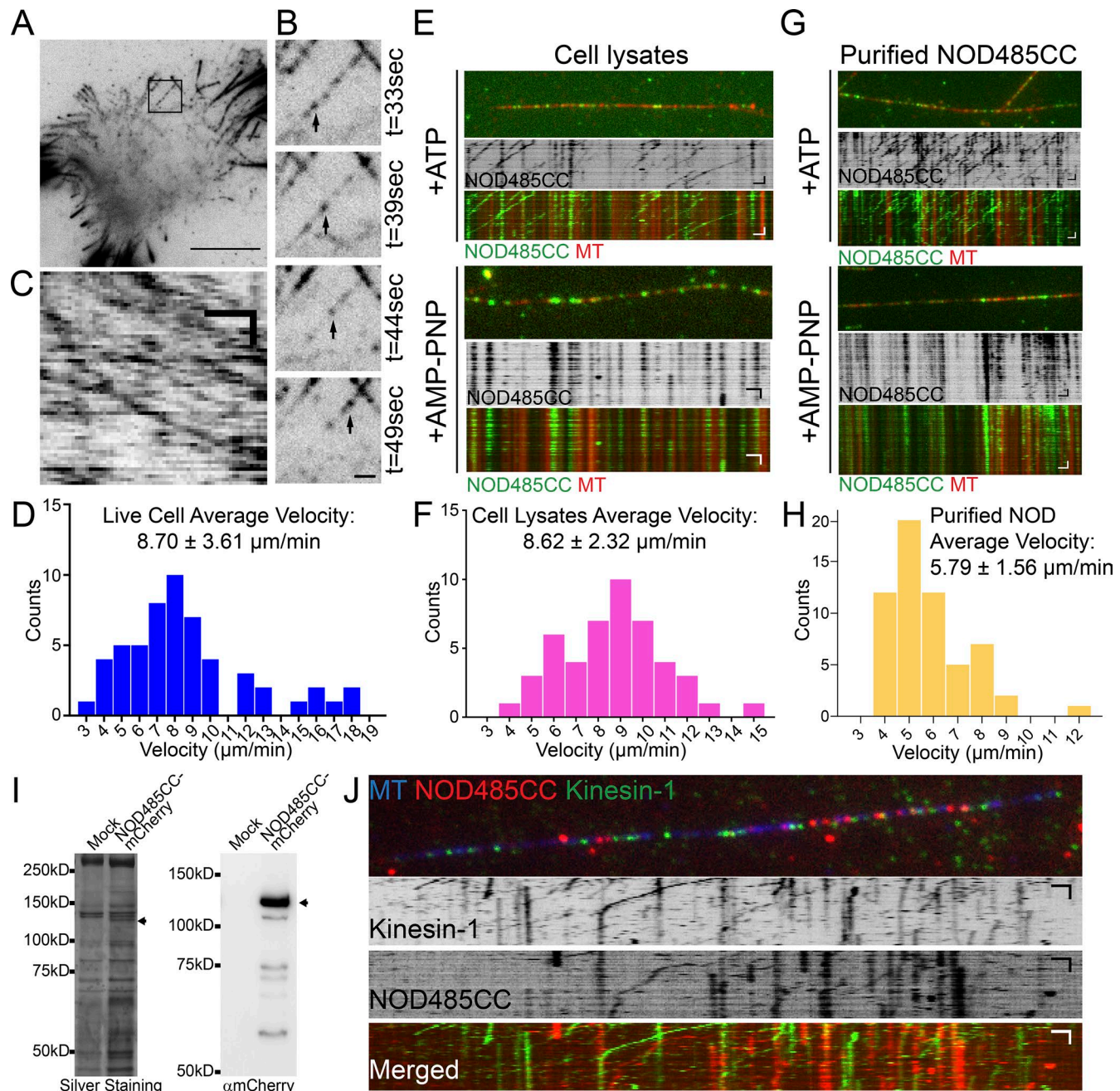


Figure 2. Dimerized NOD485 exhibits ATP-dependent, plus end-directed motility in cells and in vitro. (A) TIRF microscopy of an interphase cell expressing NOD485CC. (B) Select frames from a TIRF time-lapse zoomed on the region in the black box in A showing a motile NOD485CC dimer (marked by arrow). (C) Kymograph of NOD485CC dimer from the black box in A walking on MTs toward the cell periphery (right side of kymograph). (D) Histogram of velocities of motile NOD485CC dimers in cells, with a mean velocity of $8.70 \pm 3.61 \mu\text{m/min}$; $n = 55$. (E) TIRF microscopy of NOD dimers (green) on taxol-stabilized MTs (red) using a cell lysate from NOD485CC-mCherry-expressing cells in the presence of ATP (top) or AMP-PNP (bottom). (F) Histogram of the velocities of motile NOD485CC dimers in cell lysates, with a mean velocity of $8.62 \pm 2.32 \mu\text{m/min}$; $n = 47$. (G) TIRF microscopy of taxol-stabilized MTs (red) incubated with Strep-tagged NOD485CC-mCherry (green) purified from S2 cells in the presence of ATP (top) or AMP-PNP (bottom). (H) Histogram of the velocities of purified Strep-tagged NOD485CC puncta, with a mean velocity of $5.79 \pm 1.56 \mu\text{m/min}$; $n = 58$. (I) Silver staining of SDS-PAGE gel (left) and Western blot (right) showing the purification of NOD485CC-mCherry from *Drosophila* S2 cells and mock purification from wild-type cell extracts. Arrows indicate the NOD bands. (J) Kymograph from a TIRF time-lapse of NOD485CC lysate (red) plus purified kinesin-1-EGFP (green) on taxol-stabilized MTs (blue). Horizontal bars: 10 μm (A); 1 μm (B, C, E, G, and J). Vertical bars: 10 s (A–C, E, and G); 20 s (J). Means \pm SD.

also tracked growing plus ends (Fig. 3 K and Video 11). Spinning disc confocal imaging of cells coexpressing NOD485CC-EGFP and EB1-TagRFP-T revealed that a subset of NOD485CC puncta colocalized with EB1 tracks on MT plus ends (Fig. 4 A and Video 12).

It is worth noting that NOD often remained associated with depolymerizing MTs through a mechanism that is presently unclear, but that could be similar to the bidirectional tracking activity of CENP-E because NOD, like hKID, may possess low-affinity MT

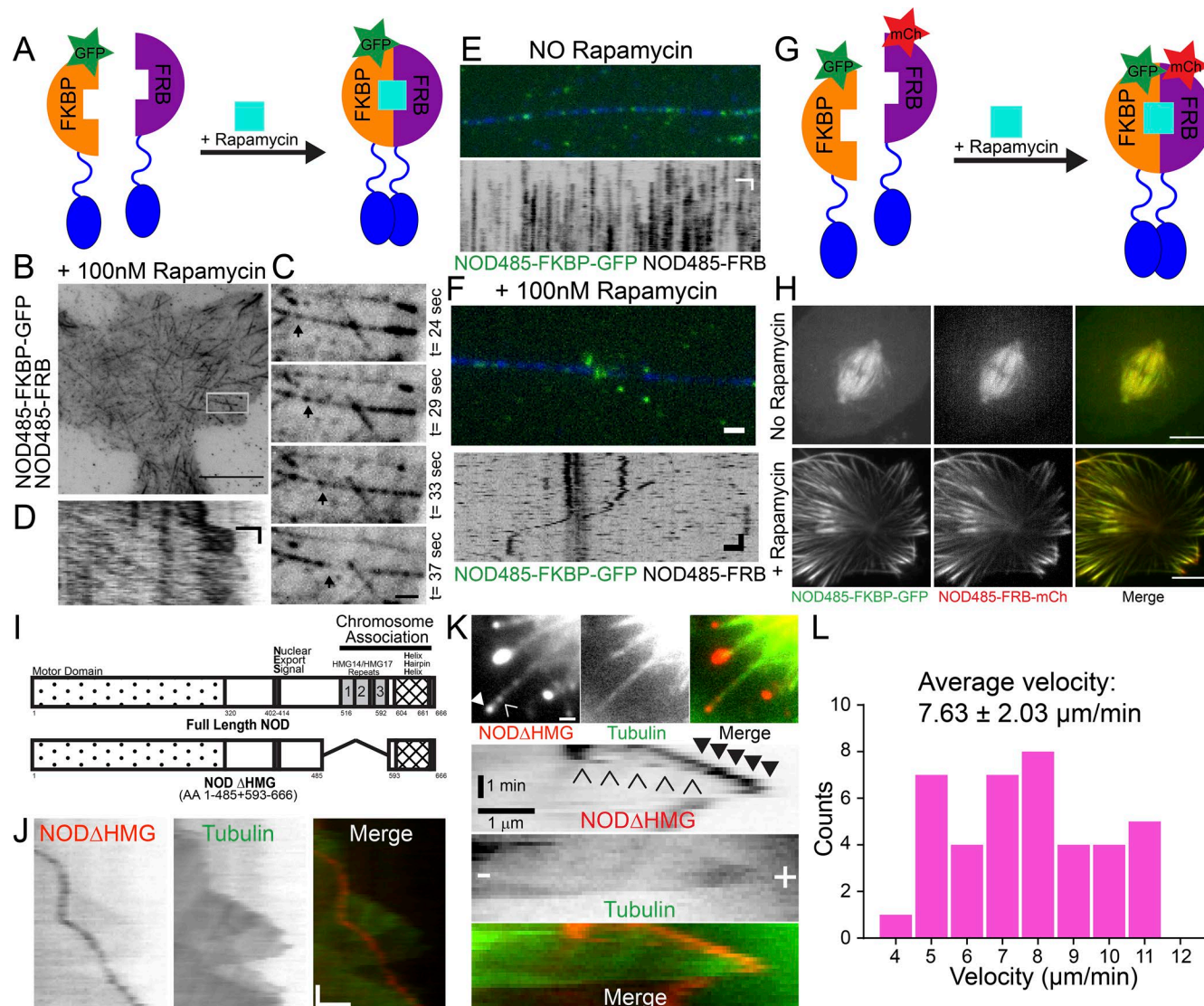


Figure 3. Chemically induced NOD dimers exhibit directional motility, and a NOD mutant lacking one of the DNA binding domains is motile and tip tracks. (A) Schematic of the rapamycin-based approach used to dimerize NOD485 molecules. (B) TIRF image of a cell expressing NOD485-FKBP-EGFP and NOD485-FRB treated with rapamycin. (C) Select frames from the region in the white box in B showing a motile NOD puncta (marked by arrows) walking toward the cell periphery (right). (D) Kymograph of dimerized NOD485 walking on a MT toward the cell periphery (right) within the white box in B. (E) TIRF assay of taxol-stabilized MTs (blue) plus lysate containing ATP prepared from cells expressing NOD485-FKBP-EGFP (green) and NOD485-FRB in the absence of rapamycin. (F) TIRF of the same cell lysate in E but in the presence of 100 nM rapamycin. A motile NOD puncta is highlighted in the kymograph. (G) Schematic of rapamycin-induced dimerization of NOD485-FKBP-EGFP and NOD485-FRB-mCherry. (H) Representative images of cells expressing NOD485-FKBP-EGFP (green) and NOD485-FRB-mCherry (red) in the absence (top) and presence (bottom) of rapamycin in which the localization pattern was the same as NOD485 and NOD485CC, respectively. (I) Schematic of NODΔHMG in which one of the chromosome-associating domains is deleted. (J) Kymograph of a NODΔHMG cluster (red) walking along MTs (green) in a cell. (K) Example of NODΔHMG cluster in a cell exhibiting two activities on the same MT (with plus and minus ends indicated in the tubulin kymograph): tip tracking (closed arrows) and plus end-directed motility (open arrows). (L) Histogram of the velocities of NODΔHMG puncta, with a mean of $7.63 \pm 2.03 \mu\text{m}/\text{min}$; $n = 37$. Horizontal bars: 10 μm (B); 1 μm (C–F, J, and K); 5 μm (H). Vertical bars: 10 s (B–F, H, and J); 1 min (K). Mean \pm SD.

binding regions outside of the motor domain (Shiroguchi et al., 2003; Gudimchuk et al., 2013). Plus end-directed NOD485CC dimers were evident behind tip-tracking NOD puncta in kymographs from NOD485CC-, EB1-expressing cells (Fig. 4 A). Given the utility of cell lysates in visualizing NOD motility, extracts from NOD485CC-EGFP-expressing cells were added to dynamic rather than taxol-stabilized MTs in an effort to better visualize NOD end tracking by TIRF microscopy in vitro. The cell-based observations were fully validated in vitro using dynamic MTs as NOD485CC clearly walked toward the faster growing plus ends

while a subpopulation of NOD485CC tip tracked on growing MT plus ends (Fig. 4 B and Video 13).

NOD's end-tracking activity combined with the observed colocalization of NOD with EB1 comets led us to next investigate if NOD and EB1 directly interact in pulldown assays using purified components. GST-EB1-TagRFP-T pulled down with MBP-NOD485CC-EGFP, but not the MBP-EGFP control protein (Fig. 4, C and D). To further characterize the NOD-EB1 interaction, we turned our attention to amino acids 325–485 because NOD485CC exhibited MT plus end-tracking activity, and NOD324CC did not

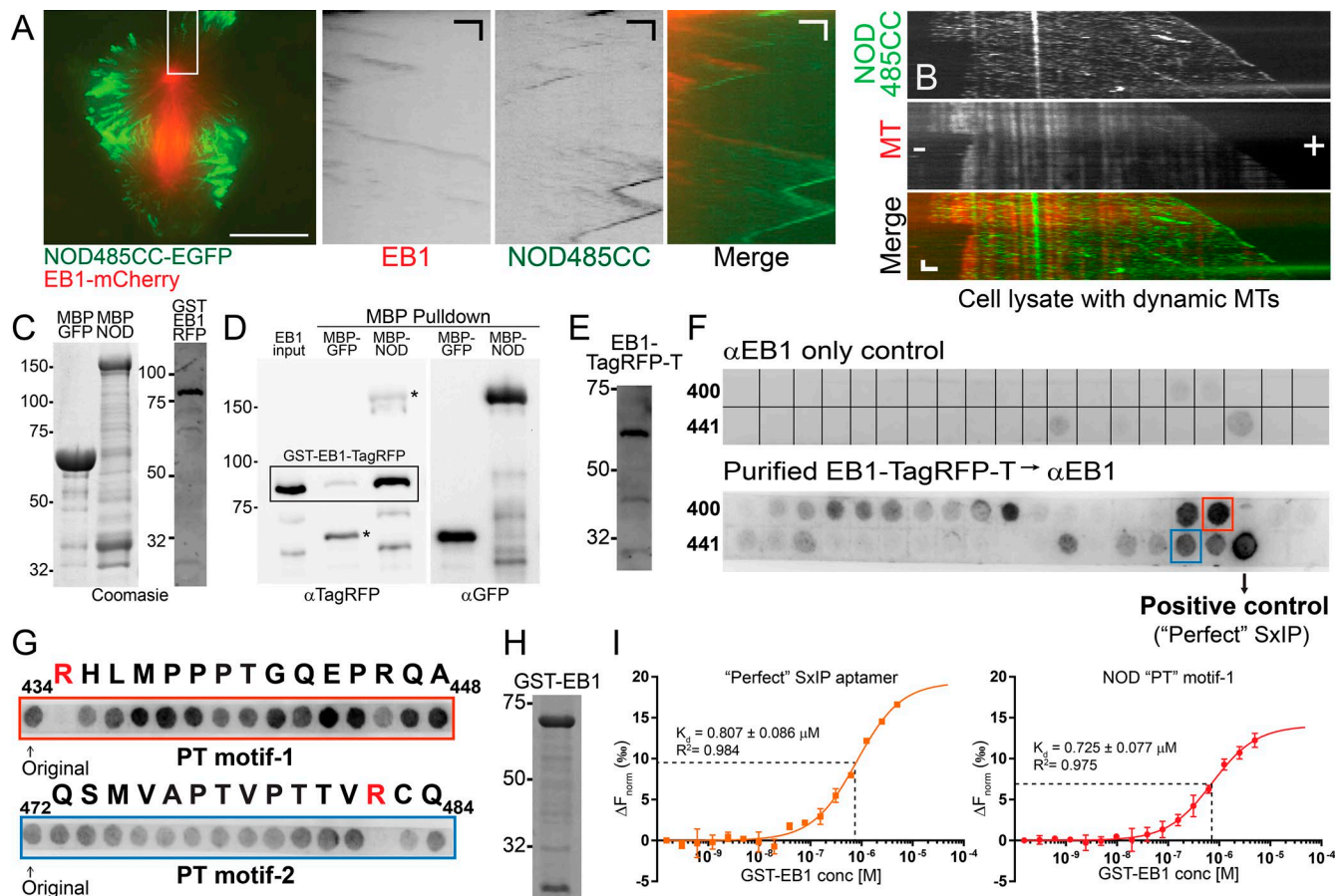


Figure 4. Dimerized NOD tip tracks on dynamic MTs and directly interacts with EB1 through a new motif. (A) A mitotic cell coexpressing NOD485CC-EGFP (green) and EB1-mCherry (red). Kymographs of dynamic astral MTs within the white box reveal subpopulations of NOD puncta tip-tracking coincident with EB1, remaining associated with depolymerizing plus ends, and walking toward the MT plus ends. (B) Kymograph of motile and tip-tracking NOD485CC (green) dimers on dynamic MTs (red, plus and minus ends labeled in MT kymograph) incubated in cell lysate and subjected to TIRF imaging. (C) Coomassie-stained SDS-PAGE gels showing purified MBP-GFP and MBP-NOD485CC-EGFP (left) and *Drosophila* GST-EB1-TagRFP-T (right) used in the pull-down assays. (D) Western blot for TagRFP of pull-down assay showing *Drosophila* GST-EB1-TagRFP-T specifically interacts with MBP-NOD485CC-EGFP, but not with MBP-EGFP (left blot). Asterisks denote α TagRFP cross-reactivity with MBP-EGFP and MBP-NOD485CC-EGFP, which were detected by Western blot with α -GFP (right blot). (E) Coomassie-stained SDS-PAGE gel showing the purified *Drosophila* EB1-TagRFP-T (GST cleaved off) used to probe the SPOT peptide arrays. (F) SPOT peptide arrays of NOD 400–485, and including a “perfect” SxIP peptide as a positive control, probed with anti-EB1 serum (control) or purified EB1-TagRFP-T followed by incubation with the anti-EB1 serum. Two peptides with positive EB1 binding are highlighted in red (PT motif-1) and blue (PT motif-2). (G) Alanine scans of the two peptides highlighted in F. (H) Coomassie-stained SDS-PAGE gel showing the purified *Drosophila* GST-EB1 used in the pull-down assays. (I) MST was done by titrating GST-EB1 while maintaining a constant concentrations of FITC-labeled “perfect” SxIP aptamer (left) or NOD “PT” motif-1 (right) resulting in measurable changes in the fluorescence signal within a temperature gradient that can be used to calculate dissociation constants (SxIP $K_d = 807 \pm 86$ nM and NOD PT motif-1 $K_d = 725 \pm 77$ nM). Error bars represent standard deviation of $n = 3$ (PT motif-1) and 2 (SxIP motif) MST runs. The K_d values are reported as mean \pm SEM. Horizontal bars: 5 μ m (A); 1 μ m in all kymographs (A and B). Vertical bars: 20 s.

(Table 1). NOD contains multiple regions that are predicted to be disordered, centered around proline (P) and threonine (T) residues between residues 430–480. These motifs are similar to unconventional EB1-binding motifs recently identified in fungal species in the *Saccharomyces cerevisiae* Kar9 motor and *Schizosaccharomyces pombe* Dis1/Tog MAP (Manatschal et al., 2016; Matsuo et al., 2016). To identify EB1-interacting regions in NOD, overlapping peptide SPOT arrays encompassing what we deemed the “PT” motifs were synthesized onto a cellulose membrane, and their interactions with purified EB1 were probed. The SPOT arrays comprised 15 amino acid peptides spanning NOD residues 430–480 with an offset of two residues and included a “perfect” SxIP aptamer as a positive control peptide (Leśniewska et al., 2014). The NOD peptides exhibiting the strongest association

with purified *Drosophila* EB1-TagRFP-T centered on the PT motifs (PT motif-1 and -2; Fig. 4, E and F).

The amino acids surrounding SxIP motifs impact their affinities for EB1 (Jiang et al., 2012; Leśniewska et al., 2014). To examine how PT-flanking amino acids contributed to EB1 binding, the peptides that exhibited the strongest association with EB1 on the array were subjected to alanine scanning (Fig. 4 G). In each peptide, mutation of a surrounding arginine (R) residue approximately three to six amino acids upstream or downstream of the PT sequence eliminated EB1 binding. The results suggest that, like the SxIP motif, neighboring basic residues contribute to the affinity of NOD PT motifs for EB1 (Honnappa et al., 2009; Leśniewska et al., 2014). During the preparation of this manuscript, the unconventional Ka9–EB1 interaction was further characterized, leading

to the designation of LxxPTPh as a novel tip-localization motif (Kumar et al., 2017). Although the PT motifs in NOD resemble the LxxPTPh motif, the compositional differences may indicate that the *Drosophila* EB1 PT motif has diverged somewhat and/or that variability in the motif still supports EB1 interactions.

Microscale thermophoresis (MST) was used to measure the binding affinity of the NOD PT motif-1 for EB1. The N terminus of either the PT motif-1 or a bona fide “perfect” SxIP peptide (positive control) was labeled with fluorescein (FITC) dye, and the movement of each fluorescently labeled peptide (fixed at 50 nM) in a temperature gradient was measured by MST while varying concentrations of unlabeled *Drosophila* GST-EB1 (Fig. 4 H). The binding affinity measured by MST for the SxIP motif was 807 nM, which is relatively close to the K_d (~570 nM) measured by isothermal titration calorimetry using the “perfect” SxIP peptide and *Drosophila* EB1 (Leśniewska et al., 2014). The affinity of the PT motif-1 for *Drosophila* EB1 was measured to be 725 nM, slightly higher than the K_d of the positive control SxIP aptamer (Fig. 4 I and Fig. S2). Thus, the NOD PT motif-1 possesses an affinity for *Drosophila* EB1 that is comparable to other bona fide SxIP motifs and higher than affinities measured for EB1-CAP-Gly interactions (Honnappa et al., 2006; Weisbrich et al., 2007).

How the *Drosophila* kinesin-10 NOD generates PEFs has long been a mystery. Prior work (Cane et al., 2013) led us to hypothesize that NOD possesses two force producing activities: (1) MT plus end-directed motility, which had never been directly demonstrated and (2) end tracking on polymerizing MTs, the mechanism of which was speculative. We demonstrate here, for the first time, that NOD exhibits plus end-directed motility in cells and in vitro and that NOD directly interacts with the tip-tracking protein EB1 via a new type of conserved MT tip localization sequence. It is noteworthy that both MT polymerization and motor activity were originally proposed as sources of the PEF when the phenomenon was first described (Rieder et al., 1986), more than 30 years later our findings reveal NOD as a molecular nexus of both force-producing mechanisms.

Materials and methods

Cell culture

Drosophila S2 cells were grown in Schneider’s medium (Life Technologies) supplemented with 10% heat-inactivated FBS and 0.5× antibiotic/antimycotic cocktail (Sigma) and maintained at 25°C. All cell lines were generated by transfecting the plasmid with Effectene Transfection Reagent system (Qiagen) following the manufacturer’s protocol. Expression of the proteins was confirmed by fluorescence microscopy. Cells expressing the constructs were selected by splitting them in the presence of 25 µg/ml Blastidicin S HCl (Thermo Fisher) and/or 250 µg/ml Hygromycin (Gibco) until cell death ceased, at which point, the cells were maintained in media without drugs. Protein expression was induced with 500 µM (high induction) or 25 µM (low induction) CuSO₄ for 16–18 h.

DNA constructs

Different NOD truncations were amplified from NOD cDNA (CG1763), with 5’ KpnI and 3’ SpeI sites and inserted into

a pMT-V5 vector with a C-terminal mCherry tag inserted between SpeI and SacII. Human kinesin-1 CC was amplified from a KIF5B construct (gift from J. Ross, University of Massachusetts, Amherst, MA) with flanking SpeI sites and inserted into the previous plasmid. A single Strep-tag (ASW SHPQFEK) was added to the C terminus by incorporating the DNA sequence (5’-GCTAGCTGGAGCCACCCGCAGTTCGAAAAA-3’) to the mCherry reverse primer. FKBP was amplified from FKBP-myc, a gift from C. Bertozzi (Stanford University, Stanford, CA; plasmid 20211; Addgene), and FRB was amplified from pEYFP-Mitotrap, a gift from M. Robinson (University of Cambridge, Cambridge, England, UK; plasmid 46942; Addgene) with flanking SpeI sites and inserted between NOD and the fluorescent protein tag. The kinesin-1 gene corresponding to amino acids 1–560 was PCR-amplified from the KIF5B construct, and the resulting PCR product, kinesin-1 (1–560 aa) was inserted between 5’ KpnI and 3’ SpeI sites of the pMT/V5-HisB vector (Invitrogen) containing the mCherry gene between 5’ SpeI and 3’ SacII sites.

Protein purification from *Drosophila* S2 cells

NOD85CC-mCherry with a C-terminal Strep-tag (-ASWSHP QFEK) was purified from *Drosophila* S2 cells. Cells were grown in 75-mm³ tissue culture flasks until confluent, and expression was induced with 500 µM CuSO₄ 24 h before harvesting. Harvested cells were resuspended in chromokinesin buffer (45 mM KCl, 36 mM Pipes, 90 mM K acetate, 5 mM MgCl₂, 1 mM EGTA, 1% Glycerol, 1 mM DTT, 1 mM PMSF, 10 µg/ml Pepstatin, 20 µg Leupeptin, 1 mM MgATP, 0.5% Triton X-100, and 100 µg/ml κ-casein) and spun at 15,000 RPM at 4°C for 15 min. The supernatant was added to washed MagStrep “type 3” XT beads (IBA), incubated at 4°C for 1 h, and subsequently eluted in chromokinesin buffer supplemented with 75 mM biotin. The purified protein was then used in TIRF assays and run on SDS-PAGE gel for silver staining and Western blot.

Live cell imaging and quantification of NOD-mCherry fluorescence using a dimeric standard

Cells were allowed to adhere to a concanavalin A-treated coverslip and mounted into a rose chamber, or plated on a concanavalin A-coated glass-bottom Petri dish. Cells were imaged on a TIRF-spinning disc system assembled on an Eclipse Ti-E inverted microscope (Nikon) equipped with a Borealis (Andor) retrofitted CSU-10 (Yokogawa) spinning disc head and two ORCA-Flash4.0 LT Digital CMOS camera (Hamamatsu) using a 100× 1.49 NA Apo differential interference contrast objective (Nikon). MetaMorph software (Molecular Devices) was used to control the imaging system. Single and dual color TIRF images were acquired at 1 and 2 s intervals, respectively. NOD velocities were measured by manually following motile puncta in cells and in vitro assays. Kymographs were generated using MetaMorph software. All graphs and statistics were done using Prism (GraphPad).

The number of molecules per mCherry puncta of NOD485CC and NODΔHMG was determined by comparing their fluorescence intensities to a known dimer standard: kinesin-1 tagged with mCherry. Before imaging, cells were induced with either 25 µM (NOD485CC) or 500 µM (NODΔHMG and kinesin-1) CuSO₄ for

16 h to induce expression. Cells coexpressing GFP- α -tubulin and Kinesin-1, NOD485CC-, or NOD Δ HMG-mCherry were each visualized sequentially via live cell TIRF microscopy using identical imaging parameters. MetaMorph software was used to measure the integrated fluorescence intensities of motile mCherry puncta by placing a 12 \times 12 pixel circular region on mCherry puncta and subtracting the local background integrated intensity from a nearby (cytosolic) 12 \times 12 circular region. Histograms and dot plots were generated using Excel software (Microsoft) and KaleidaGraph (Synergy), respectively.

TIRF-based imaging of cell lysates

Taxol-stabilized MTs were made by polymerizing 100 μ M tubulin spiked with 1% Dylite-649-labeled tubulin (Cytoskeleton) at 37°C, and stabilized with 20 μ M taxol. Cell lysate was made by plating cells on a concanavalin A-coated 100 mm Petri dish and inducing NOD expression overnight. Cells were washed once with 1 \times PBS, and lysed in 300 μ l chromokinesin buffer (45 mM KCl, 36 mM Pipes, 90 mM K acetate, 5 mM MgCl₂, 1 mM EGTA, 1% Glycerol, 1 mM DTT, 1 mM PMSF, 10 μ g/ml Pepstatin, 20 μ g Leupeptin, 1 mM MgATP, 0.5% Triton X-100, and 100 μ g/ml κ -casein). The lysate was clarified by centrifugation at 4°C for 10 min at 15,000 RPM. Flow cells were made by adhering a glass coverslip to a glass slide using two strips of double-sided tape, leaving a chamber volume of \sim 10 μ l. Antitubulin antibody YL1/2 diluted to 100 μ g/ml was first flowed into the chamber and incubated for 5 min, then blocked with 5% pluronic F-127 for 5 min. Taxol stabilized microtubules (1 μ M) were next flowed into the chamber and incubated for 5 min followed by another block with 5% pluronic F-127 for 5 min and a wash with 1 \times BRB80. Finally, cell lysates and/or purified protein were diluted to achieve a reasonable density of NOD dimers on MTs into the activation mix (45 mM KCl, 36 mM Pipes, 90 mM K acetate, 5 mM MgCl₂, 1 mM EGTA, 1% Glycerol, 1 mM DTT, 1 mM MgATP, 0.5% Pluronic F-127, 0.5% Triton X-100, and 100 μ g/ml κ -casein), flowed into the chamber, and subjected to TIRF imaging.

Bacterial protein purifications and pulldown assays

GST-EB1-TagRFP-T, MBP-NOD485CC-EGFP, and MBP-EGFP, used for all the pull down experiments, were expressed and purified from Rosetta (DE3) cells, using the following lysis buffer: 50 mM Hepes, 50 mM sucrose, 100 mM KCl, 2 mM MgCl₂, 0.5 mM EGTA, 1 mM PMSF, 1 mM DTT, and protease inhibitor cocktail. Cells were lysed using an EmulsiFlex-B30 cell disruptor (Avestin), and spun at 12,000 RPM for 30 min. The supernatant of GST-tagged proteins were then incubated with glutathione sepharose beads (GE Healthcare) and MBP-tagged proteins were incubated with amylose resin (NEB) for 1 h at 4°C; proteins were eluted with 10 mM reduced glutathione or 10 mM maltose, respectively. Protein concentrations were determined using Bradford Reagent (Bio-Rad Laboratories). Twofold molar excess of MBP-NOD485CC-EGFP, and MBP-EGFP as control was added to GST-EB1-TagRFP-T in the presence of 5 mg/ml BSA and incubated at 25°C with agitation for 1 h. Protein mixtures were then added to amylose magnetic beads (NEB) and incubated for an additional hour at 25°C. Amylose magnetic beads were preblocked with 10 mg/ml BSA for 1 h before addition of the proteins. Beads were next washed three

times with 500 μ l lysis buffer, the bound protein was eluted from the beads with 20 μ l of 1 \times SDS sample buffer, and 5 μ l of the elution samples was run on a SDS-PAGE gel for analysis next to 5% of the EB1 input and transferred to a nitrocellulose membrane for Western blot analysis. Samples were run in parallel, blotted with α -GFP antibody (Abcam) at 1:30,000 or α -TagRFP (Evrogen) at 1:5,000 separately, using the appropriate HRP secondary antibodies.

GST-EB1 used in MST assays was expressed and purified from Rosetta (DE3) cells, using the following lysis buffer: 50 mM Hepes, 50 mM sucrose, 100 mM KCl, 2 mM MgCl₂, 0.5 mM EGTA, 1 mM PMSF, 1 mM DTT, and protease inhibitor cocktail. Protocol was followed as described above.

Western blots

Proteins were loaded onto a 10% SDS-PAGE gel, run out, and transferred to a nitrocellulose membrane on the Trans-Blot Turbo transfer system (Bio-Rad Laboratories) using the pre-programmed "MIXED MW" 7 min protocol. All antibodies were diluted in TBS with 0.1% Tween and 5% milk. Antibodies used were rabbit anti-EB1 serum (gift from S. Rogers, University of North Carolina, Chapel Hill, Chapel Hill, NC) at 1:5,000, rabbit α -mCherry (PA5-34974; Thermo Fisher) at 1:5,000, chicken α -GFP (ab13970; Abcam) at 1:30,000, and rabbit α -TagRFP (AB233; Evrogen) at 1:5,000. All secondary antibodies (Jackson ImmunoResearch Laboratories, Inc.), diluted at 1:5,000, were used in conjunction with their respective primaries. Imaging of the membrane was done on a G-Box system controlled by GeneSnap software (Syngene).

Dynamic microtubules

Microtubule seeds were made by polymerizing 100 μ M of tubulin mixture (composed of unlabeled tubulin, 10% dylight-649-labeled tubulin, and 10% biotinylated tubulin) in the presence of 1 μ M GMPCPP at 37°C for 30 min. The seeds were pelleted by centrifugation at RT for 10 min at 15,000 RPM and then resuspended in warm BRB80. Seeds were sheared with a Hamilton syringe if necessary and diluted 1:100 for experiments. Chambers were created using double-sided tape and salinized coverslip with a volume of \sim 10 μ l. Biotin antibody was first flowed into the chamber and incubated for 5 min, then blocked with 5% F-127, followed by addition of the GMP CPP MT seeds. Elongation mix was then added to the chamber and imaged immediately by TIRF microscopy until MTs grew to be too long. Elongation mix: diluted cell extracts from cells expressing FP-tagged NOD485CC prepared as described above, supplemented with 30 μ M tubulin (5% dylight-649-labeled), 10 μ M GTP, 10 μ M MgATP, 50 μ M DTT, 0.2% methylcellulose, and oxygen scavenger.

Peptide arrays

SPOT peptide array membranes were generated by Biopolymers & Proteomics Laboratory at Koch Institute at Massachusetts Institute of Technology, Cambridge, MA. The membrane was first blocked with blocking buffer (1 \times blocking buffer [Sigma], 1 \times TBS, and 0.05% sucrose) overnight at RT, then incubated with 5 μ g/ml purified EB1-TagRFP-T for 3 h at RT, then washed three

times with 1× TBS. Protein binding was detected using anti-EB1 serum diluted at 1:1,000 in the blocking buffer, followed by three-times wash with 1× TBS and incubation with the corresponding HRP secondary. The control blot of the SPOT array was blocked overnight then washed three times with 1× TBS before incubating with the anti-EB1 serum diluted at 1:1,000 in the blocking buffer.

MST

We elected to use microscale thermophoresis to determine the binding affinity of NOD “PT” peptides to EB1 because this technique yields quick and accurate K_d values with small amounts of fluorescently labeled samples. Additionally, this technique also allows for use of any buffer, allowing us to keep EB1 and NOD peptides in the most optimal buffer conditions. NOD “PT” motif-1 and perfect SxIP aptamer was N-terminal labeled with FITC by incubating fivefold molar excess of the dye to the peptide in 1× PBS and incubated at RT for 2 h. The free dye was removed from the labeled peptide through ZipTip C18 (EMD-Millipore). Peptide concentration after labeling was determined by 205-nm absorbance, with the extinction coefficient defined according to [Anthis and Clore \(2013\)](#). A series of GST-EB1 titrations were added to 50 nM of labeled peptide in the presence of 0.5% tween, filled into 16 standard MST capillary tubes (NanoTemper Technologies) for a single experiment, then subjected to thermophoresis measurements in a Monolith NT.115 (NanoTemper). Fluorescence was recorded for 20 s using 20% laser power. F_{norm} (%) is the change in fluorescence of the “hot” region at 5 s in respect to the “cold” region at time = 0. The dissociation constants were calculated by plotting ΔF_{norm} (change of F_{norm} in respect to the zero EB1 concentration) against GST-EB1 concentrations on a log scale X axis, and fitting the data using a Michaelis-Menten equation in Prism (GraphPad).

Online supplemental material

Fig. S1 shows quantification of NOD-mCherry signals compared with a dimeric kinesin-1 standard. Fig. S2 shows the raw data from microscale thermophoresis measurements. Video 1 is TIRF imaging of NOD485CC-mCherry in an interphase cell. Videos 2 and 3 depict TIRF microscopy of NOD485CC dimers in cell extracts on taxol-stabilized MTs in the presence of ATP and AMP-PNP, respectively. Videos 4 and 5 depict TIRF microscopy of purified Strep-tagged NOD485CC on taxol-stabilized MTs in the presence of ATP and AMP-PNP, respectively. Video 6 shows TIRF microscopy of NOD485CC-mCherry cell extracts plus purified kinesin-1-EGFP. Video 7 shows TIRF imaging of an interphase S2 cell coexpressing NOD485FKBP-EGFP and NOD485-FRB. Videos 8 and 9 show TIRF imaging of extracts prepared from cells coexpressing NOD485FKBP-EGFP and NOD485-FRB without and with rapamycin, respectively. Video 10 depicts two-color TIRF imaging of an S2 cell expressing NODΔHMG-mCherry and EGFP- α -tubulin. Video 11 shows two-color wide-field imaging of an S2 cell expressing NODΔHMG-mCherry and EGFP- α -tubulin. Video 12 depicts spinning disc confocal imaging of a mitotic S2 cell coexpressing NOD485CC-EGFP and EB1-TagRFP-T. Video 13 shows TIRF imaging of lysate from cells expressing NOD-485CC-mCherry with dynamic microtubules.

Acknowledgments

We thank Jason Stumpff (University of Vermont, Burlington, VT) for sharing insights on buffer conditions for in vitro motility assays with chromokinesins. We also acknowledge Steve Rogers (University of North Carolina, Chapel Hill, Chapel Hill, NC) for sharing anti-EB1 serum and Jennifer Ross (University of Massachusetts, Amherst, Amherst, MA) for purified kinesin-1-EGFP and kinesin K560 plasmid. Microscale thermophoresis data were obtained at the University of Massachusetts Biophysical Characterization Facility.

This work was supported by a National Institutes of Health grant (GM107026) to T.J. Maresca and by a March of Dimes Foundation grant to T.J. Maresca (grant 5-FY13-205).

The authors declare no competing financial interests.

Author contributions: A.A. Ye contributed to conceptualization, formal analysis, investigation, methodology, resource development, data validation, visualization, and original drafting, as well as review and editing of the manuscript. V. Verma contributed to fluorescence quantification of motile NOD puncta, which involved formal analysis, investigation, resource development, validation of NOD motility in cells, visualization of related data, and writing and editing related materials and methods. T.J. Maresca conceptualized the project, acquired financial support, administered the project, supervised researchers, contributed to data visualization, and reviewed and edited the manuscript.

Submitted: 16 August 2017

Revised: 14 March 2018

Accepted: 25 May 2018

References

- Afshar, K., N.R. Barton, R.S. Hawley, and L.S. Goldstein. 1995a. DNA binding and meiotic chromosomal localization of the *Drosophila* nod kinesin-like protein. *Cell*. 81:129–138. [https://doi.org/10.1016/0092-8674\(95\)90377-1](https://doi.org/10.1016/0092-8674(95)90377-1)
- Afshar, K., J. Scholey, and R.S. Hawley. 1995b. Identification of the chromosome localization domain of the *Drosophila* nod kinesin-like protein. *J. Cell Biol.* 131:833–843. <https://doi.org/10.1083/jcb.131.4.833>
- Anthis, N.J., and G.M. Clore. 2013. Sequence-specific determination of protein and peptide concentrations by absorbance at 205 nm. *Protein Sci.* 22:851–858. <https://doi.org/10.1002/pro.2253>
- Antonio, C., I. Ferby, H. Wilhelm, M. Jones, E. Karsenti, A.R. Nebreda, and I. Vernos. 2000. Xkid, a chromokinesin required for chromosome alignment on the metaphase plate. *Cell*. 102:425–435. [https://doi.org/10.1016/S0092-8674\(00\)00048-9](https://doi.org/10.1016/S0092-8674(00)00048-9)
- Bieling, P., I. Kronja, and T. Surrey. 2010. Microtubule motility on reconstituted meiotic chromatin. *Curr. Biol.* 20:763–769. <https://doi.org/10.1016/j.cub.2010.02.067>
- Bringmann, H., G. Skiniotis, A. Spilker, S. Kandels-Lewis, I. Vernos, and T. Surrey. 2004. A kinesin-like motor inhibits microtubule dynamic instability. *Science*. 303:1519–1522. <https://doi.org/10.1126/science.1094838>
- Brouhard, G.J., and A.J. Hunt. 2005. Microtubule movements on the arms of mitotic chromosomes: polar ejection forces quantified in vitro. *Proc. Natl. Acad. Sci. USA*. 102:13903–13908. <https://doi.org/10.1073/pnas.0506017102>
- Buchan, D.W., F. Minneci, T.C. Nugent, K. Bryson, and D.T. Jones. 2013. Scalable web services for the PSIPRED Protein Analysis Workbench. *Nucleic Acids Res.* 41(W1):W349–57. <https://doi.org/10.1093/nar/gkt381>
- Cai, D., K.J. Verhey, and E. Meyhöfer. 2007. Tracking single Kinesin molecules in the cytoplasm of mammalian cells. *Biophys. J.* 92:4137–4144. <https://doi.org/10.1529/biophysj.106.100206>
- Cane, S., A.A. Ye, S.J. Luks-Morgan, and T.J. Maresca. 2013. Elevated polar ejection forces stabilize kinetochore-microtubule attachments. *J. Cell Biol.* 200:203–218. <https://doi.org/10.1083/jcb.201211119>

- Carpenter, A.T. 1973. A meiotic mutant defective in distributive disjunction in *Drosophila melanogaster*. *Genetics*. 73:393–428.
- Cochran, J.C., C.V. Sindelar, N.K. Mulko, K.A. Collins, S.E. Kong, R.S. Hawley, and F.J. Kull. 2009. ATPase cycle of the nonmotile kinesin NOD allows microtubule end tracking and drives chromosome movement. *Cell*. 136:110–122. <https://doi.org/10.1016/j.cell.2008.11.048>
- Cui, W., and R.S. Hawley. 2005. The HhH2/NDD domain of the *Drosophila* Nod chromokinesin-like protein is required for binding to chromosomes in the oocyte nucleus. *Genetics*. 171:1823–1835. <https://doi.org/10.1534/genetics.105.047464>
- Cui, W., L.R. Sproul, S.M. Gustafson, H.J. Matthies, S.P. Gilbert, and R.S. Hawley. 2005. *Drosophila* Nod protein binds preferentially to the plus ends of microtubules and promotes microtubule polymerization in vitro. *Mol. Biol. Cell*. 16:5400–5409. <https://doi.org/10.1091/mbc.e05-06-0582>
- Davies, T., N. Kodera, G.S. Kaminski Schierle, E. Rees, M. Erdelyi, C.F. Kaminski, T. Ando, and M. Mishima. 2015. CYK4 promotes antiparallel microtubule bundling by optimizing MKLP1 neck conformation. *PLoS Biol.* 13:e1002121. <https://doi.org/10.1371/journal.pbio.1002121>
- Funabiki, H., and A.W. Murray. 2000. The *Xenopus* chromokinesin Xkid is essential for metaphase chromosome alignment and must be degraded to allow anaphase chromosome movement. *Cell*. 102:411–424. [https://doi.org/10.1016/S0092-8674\(00\)00047-7](https://doi.org/10.1016/S0092-8674(00)00047-7)
- Goldstein, L.S. 1993. With apologies to scheherazade: tails of 1001 kinesin motors. *Annu. Rev. Genet.* 27:319–351. <https://doi.org/10.1146/annurev.ge.27.120193.001535>
- Goshima, G., and R.D. Vale. 2003. The roles of microtubule-based motor proteins in mitosis. *J. Cell Biol.* 162:1003–1016. <https://doi.org/10.1083/jcb.200303022>
- Gudimchuk, N., B. Vitre, Y. Kim, A. Kiyatkin, D.W. Cleveland, F.I. Ataullakhanov, and E.L. Grishchuk. 2013. Kinetochore kinesin CENP-E is a processive bi-directional tracker of dynamic microtubule tips. *Nat. Cell Biol.* 15:1079–1088. <https://doi.org/10.1038/ncb2831>
- Honnappa, S., O. Okhrimenko, R. Jaussi, H. Jawhari, I. Jelesarov, F.K. Winkler, and M.O. Steinmetz. 2006. Key interaction modes of dynamic +TIP networks. *Mol. Cell*. 23:663–671. <https://doi.org/10.1016/j.molcel.2006.07.013>
- Honnappa, S., S.M. Gouveia, A. Weisbrich, F.F. Damberger, N.S. Bhavesh, H. Jawhari, I. Grigoriev, F.J.A. van Rijssel, R.M. Buey, A. Lawera, et al. 2009. An EB1-binding motif acts as a microtubule tip localization signal. *Cell*. 138:366–376. <https://doi.org/10.1016/j.cell.2009.04.065>
- Hu, C.K., M. Coughlin, C.M. Field, and T.J. Mitchison. 2011. KIF4 regulates midzone length during cytokinesis. *Curr. Biol.* 21:815–824. <https://doi.org/10.1016/j.cub.2011.04.019>
- Jiang, K., G. Toedt, S. Montenegro Gouveia, N.E. Davey, S. Hua, B. van der Vaart, I. Grigoriev, J. Larsen, L.B. Pedersen, K. Bezstarosti, et al. 2012. A Proteome-wide screen for mammalian SxIP motif-containing microtubule plus-end tracking proteins. *Curr. Biol.* 22:1800–1807. <https://doi.org/10.1016/j.cub.2012.07.047>
- Klopfenstein, D.R., and R.D. Vale. 2004. The lipid binding pleckstrin homology domain in UNC-104 kinesin is necessary for synaptic vesicle transport in *Caenorhabditis elegans*. *Mol. Biol. Cell*. 15:3729–3739. <https://doi.org/10.1091/mbc.e04-04-0326>
- Klopfenstein, D.R., M. Tomishige, N. Stuurman, and R.D. Vale. 2002. Role of phosphatidylinositol(4,5)bisphosphate organization in membrane transport by the Unc104 kinesin motor. *Cell*. 109:347–358. [https://doi.org/10.1016/S0092-8674\(02\)00708-0](https://doi.org/10.1016/S0092-8674(02)00708-0)
- Kumar, A., C. Manatschal, A. Rai, I. Grigoriev, M.S. Degen, R. Jaussi, I. Kretschmar, A.E. Prota, R. Volkmer, R.A. Kammerer, et al. 2017. Short Linear Sequence Motif LxxPTPh Targets Diverse Proteins to Growing Microtubule Ends. *Structure*. 25:924–932.e4. <https://doi.org/10.1016/j.str.2017.04.010>
- Leśniewska, K., E. Warbrick, and H. Ohkura. 2014. Peptide aptamers define distinct EB1- and EB3-binding motifs and interfere with microtubule dynamics. *Mol. Biol. Cell*. 25:1025–1036. <https://doi.org/10.1091/mbc.e13-08-0504>
- Levesque, A.A., and D.A. Compton. 2001. The chromokinesin Kid is necessary for chromosome arm orientation and oscillation, but not congression, on mitotic spindles. *J. Cell Biol.* 154:1135–1146. <https://doi.org/10.1083/jcb.200106093>
- Lupas, A., M. Van Dyke, and J. Stock. 1991. Predicting coiled coils from protein sequences. *Science*. 252:1162–1164. <https://doi.org/10.1126/science.252.5009.1162>
- Manatschal, C., A.M. Farcas, M.S. Degen, M. Bayer, A. Kumar, C. Landgraf, R. Volkmer, Y. Barral, and M.O. Steinmetz. 2016. Molecular basis of Kar9-Bim1 complex function during mating and spindle positioning. *Mol. Biol. Cell*. mbc.E16-07-0552. <https://doi.org/10.1091/mbc.E16-07-0552>
- Mann, B.J., S.K. Balchand, and P. Wadsworth. 2017. Regulation of Kif15 localization and motility by the C-terminus of TPX2 and microtubule dynamics. *Mol. Biol. Cell*. 28:65–75. <https://doi.org/10.1091/mbc.e16-06-0476>
- Matsuo, Y., S.P. Maurer, M. Yukawa, S. Zakian, M.R. Singleton, T. Surrey, and T. Toda. 2016. An unconventional interaction between Dis1/TOG and Mal3/EB1 in fission yeast promotes the fidelity of chromosome segregation. *J. Cell Sci.* 129:4592–4606.
- Matthies, H.J., R.J. Baskin, and R.S. Hawley. 2001. Orphan kinesin NOD lacks motile properties but does possess a microtubule-stimulated ATPase activity. *Mol. Biol. Cell*. 12:4000–4012. <https://doi.org/10.1091/mbc.12.4000>
- Rieder, C.L., E.A. Davison, L.C. Jensen, L. Cassimeris, and E.D. Salmon. 1986. Oscillatory movements of monooriented chromosomes and their position relative to the spindle pole result from the ejection properties of the aster and half-spindle. *J. Cell Biol.* 103:581–591. <https://doi.org/10.1083/jcb.103.2.581>
- Shiroguchi, K., M. Ohsugi, M. Edamatsu, T. Yamamoto, and Y.Y. Toyoshima. 2003. The second microtubule-binding site of monomeric kid enhances the microtubule affinity. *J. Biol. Chem.* 278:22460–22465. <https://doi.org/10.1074/jbc.M212274200>
- Stumpff, J., M. Wagenbach, A. Franck, C.L. Asbury, and L. Wordeman. 2012. Kif18A and chromokinesins confine centromere movements via microtubule growth suppression and spatial control of kinetochore tension. *Dev. Cell*. 22:1017–1029. <https://doi.org/10.1016/j.devcel.2012.02.013>
- Takagi, J., T. Itabashi, K. Suzuki, and S. Ishiwata. 2013. Chromosome position at the spindle equator is regulated by chromokinesin and a bipolar microtubule array. *Sci. Rep.* 3:2808. <https://doi.org/10.1038/srep02808>
- Theurkauf, W.E., and R.S. Hawley. 1992. Meiotic spindle assembly in *Drosophila* females: behavior of nonexchange chromosomes and the effects of mutations in the nod kinesin-like protein. *J. Cell Biol.* 116:1167–1180. <https://doi.org/10.1083/jcb.116.5.1167>
- Tokai-Nishizumi, N., M. Ohsugi, E. Suzuki, and T. Yamamoto. 2005. The chromokinesin Kid is required for maintenance of proper metaphase spindle size. *Mol. Biol. Cell*. 16:5455–5463. <https://doi.org/10.1091/mbc.e05-03-0244>
- Tomishige, M., D.R. Klopfenstein, and R.D. Vale. 2002. Conversion of Unc104/KIF1A kinesin into a processive motor after dimerization. *Science*. 297:2263–2267. <https://doi.org/10.1126/science.1073386>
- Vale, R.D., and R.A. Milligan. 2000. The way things move: looking under the hood of molecular motor proteins. *Science*. 288:88–95. <https://doi.org/10.1126/science.288.5463.88>
- Wandke, C., M. Barisic, R. Sigl, V. Rauch, F. Wolf, A.C. Amaro, C.H. Tan, A.J. Pereira, U. Kutay, H. Maiato, et al. 2012. Human chromokinesins promote chromosome congression and spindle microtubule dynamics during mitosis. *J. Cell Biol.* 198:847–863. <https://doi.org/10.1083/jcb.201106060>
- Weisbrich, A., S. Honnappa, R. Jaussi, O. Okhrimenko, D. Frey, I. Jelesarov, A. Akhmanova, and M.O. Steinmetz. 2007. Structure-function relationship of CAP-Gly domains. *Nat. Struct. Mol. Biol.* 14:959–967. <https://doi.org/10.1038/nsmb1291>
- Yajima, J., M. Edamatsu, J. Watai-Nishii, N. Tokai-Nishizumi, T. Yamamoto, and Y.Y. Toyoshima. 2003. The human chromokinesin Kid is a plus end-directed microtubule-based motor. *EMBO J.* 22:1067–1074. <https://doi.org/10.1093/emboj/cdg102>
- Zhang, P., and R.S. Hawley. 1990. The genetic analysis of distributive segregation in *Drosophila melanogaster*. II. Further genetic analysis of the nod locus. *Genetics*. 125:115–127.
- Zhang, P., B.A. Knowles, L.S. Goldstein, and R.S. Hawley. 1990. A kinesin-like protein required for distributive chromosome segregation in *Drosophila*. *Cell*. 62:1053–1062. [https://doi.org/10.1016/0092-8674\(90\)90383-P](https://doi.org/10.1016/0092-8674(90)90383-P)